Electronic Supplementary Material (ESI) for ChemComm.

Robust Dual-Cross-Linked Networks Enable Stable Silicon Anodes

Yun Liu,[#a,b] Hui Zhang*[#a] Jinrong Zeng,[b] Wenlu Sun,[b] Hao Qian,[b] Fang Fu,[b] Hongcun Bai,[a] Huabin Kong,*[b] Hongwei Chen*[b]

Y. Liu, Dr. H. Zhang, Prof. H. Bai

[a]National Key Laboratory of High-efficiency Utilization of Coal and Green Chemical Engineering, Ningxia University, Yinchun, 750021, China

J. Zeng, W. Sun, Prof. H. Qian, Prof. F. Fu, Dr. H. Kong, Prof. H. Chen

[b]College of Materials Science and Engineering, Huaqiao University, Xiamen, 361021, China

#These authors contributed equally to this work

Corresponding authors:

*Hui Zhang, E-mail: zhang_hui0058@nxu.edu.cn

*Huabin Kong, E-mail: konghuabin@hqu.edu.cn

*Hongwei Chen, E-mail: hwchen@hqu.edu.cn

EXPERIMENTAL SECTION

***Synthesis of $Ti_3C_2T_x$ (MX)*:** 2 g Ti_3AlC_2 powders (400 mesh,11 company) was slowly added to a mixture of 2 g lithium fluoride (LiF, alladin) and 40 mL 9 M hydrochloric acid (HCl) under stirring at 40 °C for 24 h to exfoliate the Al layers. Then, the obtained product was washed by deionized water and centrifuged several times until the pH of the supernatant reached 6. After that, anhydrous ethanol was added and ultrasonic for 1 h. Next, deionized water was used as solvent, ultrasonic and centrifugation for three times. Finally, the product was obtained *via* freeze-drying.

***Synthesis of Blank electrode*:** 80 mg nano-Si and 10 mg conductive acetylene black(AB) were mechanically milled for 30 min. Then 1 wt% $[C_6H_7O_2(OH)_2CH_2COONa]_n$ (CMC) solution was added and magnetic stirring for 4 h to obtain a homogeneous mixture. The resulting slurry was coated on Cu foil with a thickness of 100 μm and dried in a vacuum oven at 80 °C for 12 h.

***Synthesis of Micro-PBUs*.** Firstly, nano-Si and conductive acetylene black were mechanically milled for 30 min. Then, 1.5 wt% CMC dispersion and 1 wt% thiourea (SN) dispersion (molar ratio: CMC and SN = 1:1) were added in above mixture (mass ratio: Si: acetylene black: CMC+SN = 8:1:1) and magnetic stirring for 2 h. Finally, the maillard reaction was induced by stirring under argon atmosphere at 120°C. The Micro-PBUs electrode was directly coated on Cu foil.

***Synthesis of Macro-PBUs*.** The Si-PBUs and MX were mechanically milled. Then, 1.5 wt% CMC dispersion and 1 wt% thiourea (SN) dispersion (molar ratio: CMC and SN = 1:1) were added in above mixture (mass ratio: Si: MX: CMC+SN = 8:1:1) and magnetic stirring for 2 h. Finally, the secondary crosslinking reaction was carried out in argon atmosphere at 120°C. The Macro-PBUs electrode was directly coated on Cu foil.

Synthesis of Macro-PBUs-W-MX: The Si-PBUs was mechanically milled. Then, 1.5 wt% CMC dispersion and 1 wt% thiourea (SN) dispersion (molar ratio: CMC and SN = 1:1) were added in Si-PBUs (mass ratio: Si-PBUs: CMC+SN = 8:1) and magnetic stirring for 2 h. Finally, the secondary cross-linking was carried out in argon atmosphere at 120°C. The Macro-PBUs-W-MX electrode was directly coated on Cu foil.

Material Characterizations

The composition and purity of the material were characterized by X-ray diffraction (XRD) on Bruker D8-advance X-ray diffractometer with Cu-Kα radiation (λ=1.5418 Å), using an operating voltage and current of 40 kV and 40 mA. SEM images were obtained with a FEI Quanta 400 FEG equipped with EDX (Apollo 40 SDD) operated at 10 kV. TEM images were recorded using a Tecnai G2 F20 S-TWIN at 200 kV. TEM images were recorded using a Tecnai G2 F20 S-TWIN at 200 kV. Combined DTA-TG measurement was conducted in a SETARAM DSC−141 at a heating rate of 10 K min^{-1} in air atmosphere. FTIR spectrums were collected using a Thermoscientific Nicolet 6700 spectrometer.

Electrochemical Measurements

The electrochemical evaluation was performed on 2032-type coin cells. The Blank, Micro-PBUs, Macro-PBUs, and Macro-PBUs-W-MX electrodes were cut into small disks with diameter of 12 mm and then directly used as the working electrodes. The average mass loading of active materials was 1.0-1.2 mg cm^{-2}. For the semi-battery assembly, we performed the operation in an argon glove box with lithium plate as the electrode, 1 M $LiPF_6$, EC:DEC (Volume ratio1:1), 0.5wt%VC, and 7.5wt%FEC as the electrolyte. The cyclic voltammetry (CV) and electrochemical impendence spectroscopy (EIS) measurements were performed on CHI760E electrochemical workstation with a voltage range from 3 to 0.01 V at a scanning rate of 0.2 mV s^{-1}. The galvanostatic charge/discharge measurements were performed on a battery testing system (NEWARE technology Ltd. Shenzhen) with a voltage of 0.01−1.0 V. The electrodes were activated for 5 cycles at a current density of 500 mA g^{-1}.

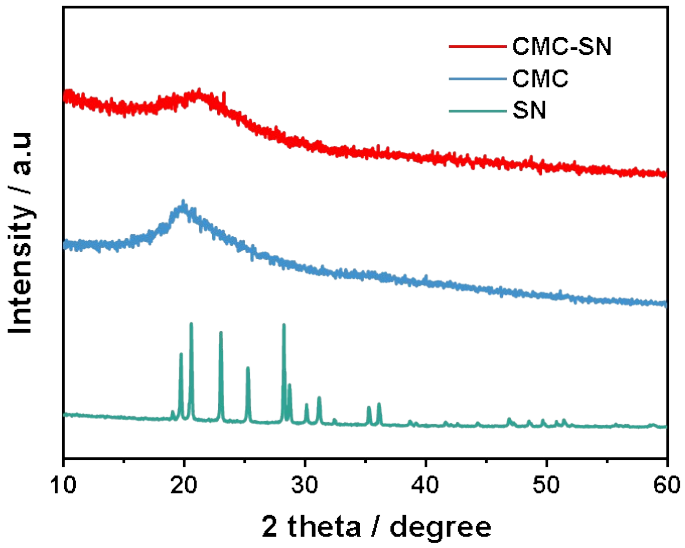

Fig. S1. XRD patterns of CMC-SN, CMC, and SN.

The Maillard reaction essentially refers to the carbonyl amino condensation reaction, occurs at 120°C-150°C. As shown in Fig. S1, the main diffraction peak of CMC at about 20° broadens and the diffraction peak of SN appeared in the curve of CMC-SN. Combined with the result of FTIR spectra (Fig. 1c), it can be proved that Maillard reaction occurred between CMC and SN

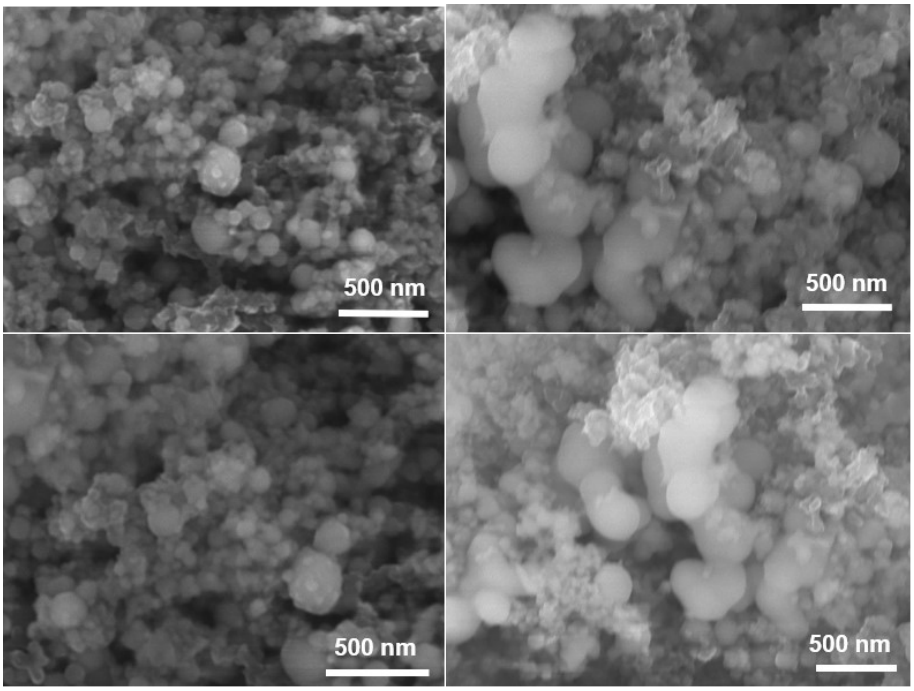

Fig. S2. SEM images of Micro-PBUs.

To prevent CMC-SN coating on the surface of Si particles leads to low conductivity issues, AB was added during the primary solidification. As shown in Fig. S2, silicon nanoparticles are surrounded by AB without agglomeration and is evenly dispersed due to the adhesive action of CMC-SN.

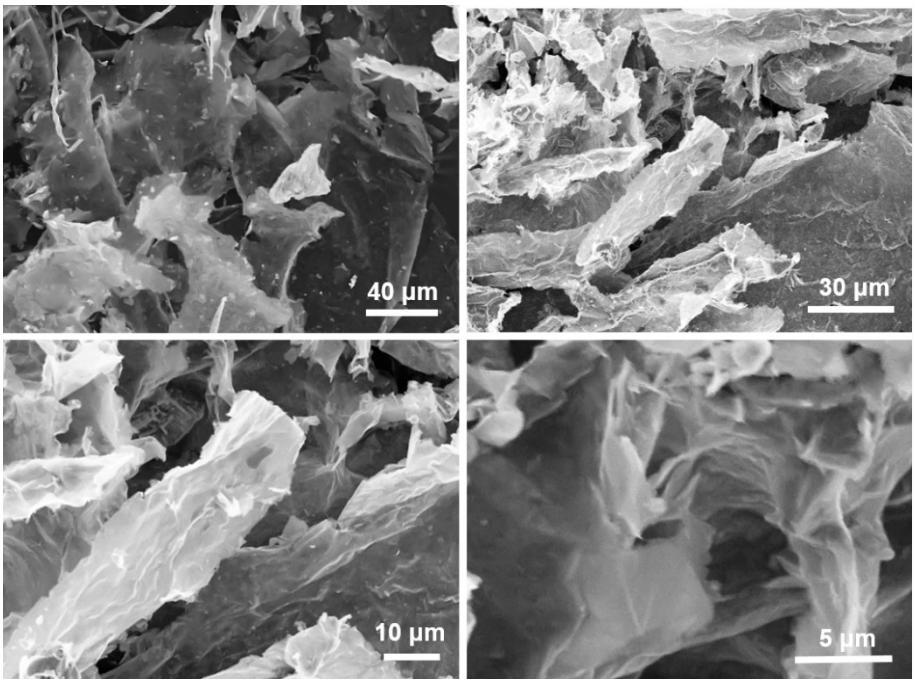

Fig. S3. SEM images of MX

Fig. S3 shows that MX has a large-area continuous layered structure. The large specific surface area of MX is conducive to coating silicon, thereby forming 3D conducting frame structures.

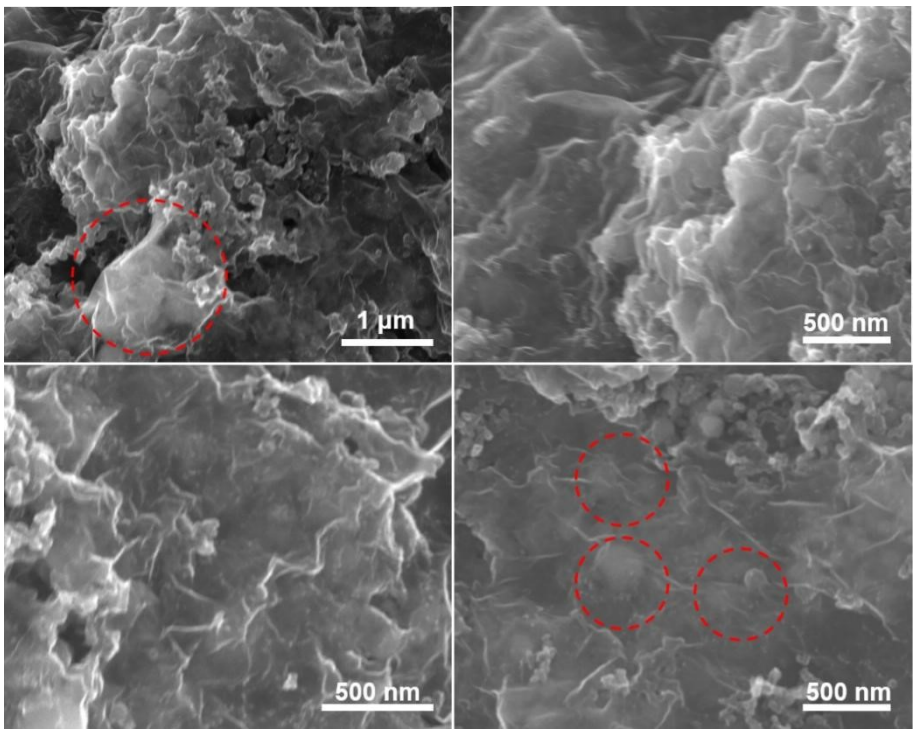

Fig. S4. SEM images of Macro-PBUs.

Macro-PBUs mainly exhibits a sheet-like structure of MX and a large number of Si-PBUs are encapsulated into the MX (**Fig. 1f**, **g** and **S4**). It can be seen that the combination between Si particles and MX is very tightly, which may be due to the bonding effect between the surface functional groups of MX and Si. The 3D conductive framework of Macro-PBUs is beneficial to alleviate the volume expansion of Si and enhance the structural stability.

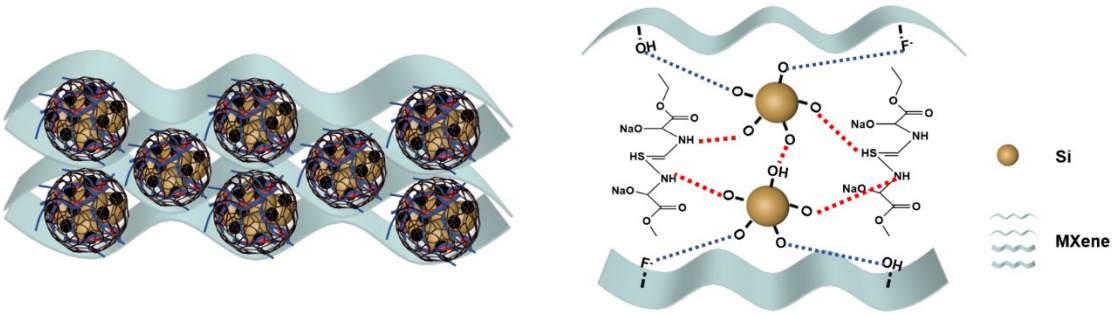

Fig. S5. (a) Structure diagram visualization of Macro-PBUs. (b) The bonding situation inside the Macro-PBUs.

According to the SEM and TEM images of Macro-PBUs, a visualization view was designed and displayed in Fig. S5a. As shown in Fig. S5b, the surface of MX has electronegative surface functional groups such as F^- and –OH, which can be bond with the functional groups on the surface of Si. Therefore, active substances are tightly bound to each other through the strong cross-links, forming the 3D conductive framework. The 3D conductive framework can alleviate the volume deformation of Si and boost the electron conduction during cycling.

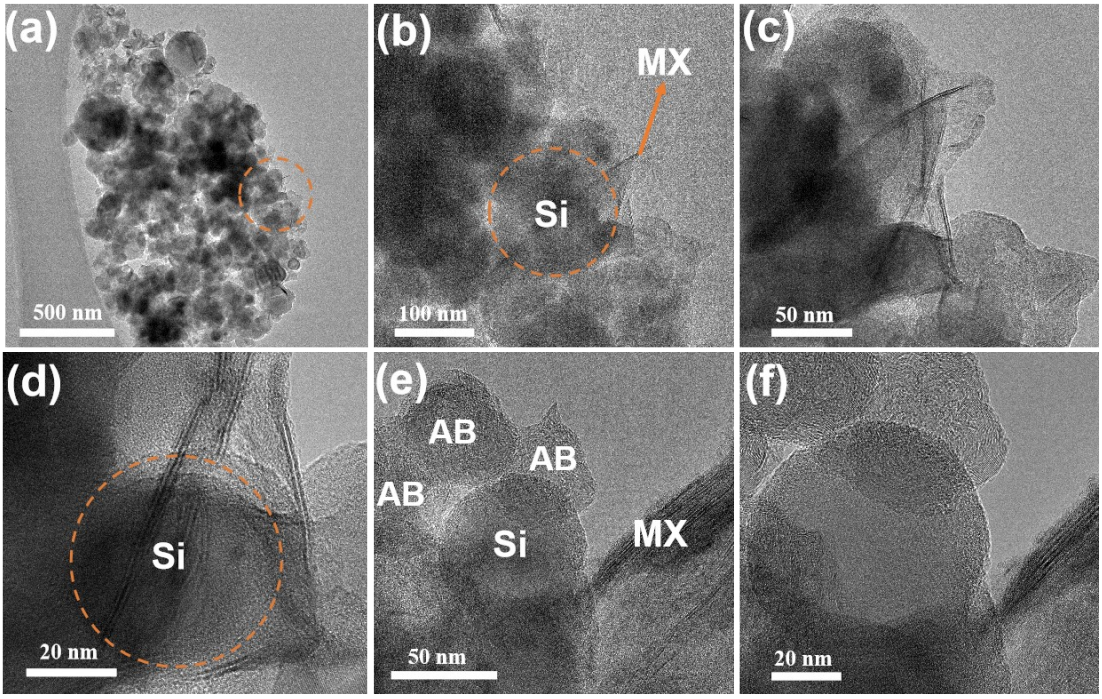

Fig. S6. (a, b) TEM images of Macro-PBUs, (c-f) HRTEM images of Macro-PBUs.

As displayed in Fig. S6, Macro-PBUs are mainly composed of Si nanoparticles, MX, and AB particles. Notably, AB particles encircle Si nanoparticles and establish a robust connection, forming Micro-PBUs through a cross-linked polymer binder. In addition, multiple Micro-PBUs are encapsulated by MX and form Macro-PBUs. It can be seen from the HRTEM images that the Micro-PBUs is also closely connected to MX by crosslinking chemistry. This secondary cross-linked polymer network may not only reinforce the complex structure but also establish vital conductive pathways across the electrode, thus enabling high capacity utilization.

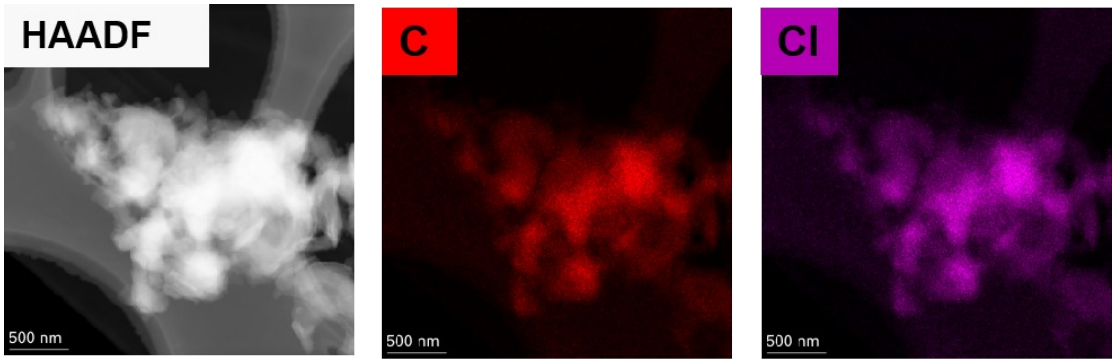

Fig. S7. EDX mapping of Macro-PBUs.

Macro-PBUs was sliced and tested for EDX mapping. As shown in Fig. S7, the uniform distribution of the five elements at the cross-section demonstrates good contact between MX and Si, which is consistent with the results of SEM. This close contact can greatly improve the structural stability and conductivity of electrode material.

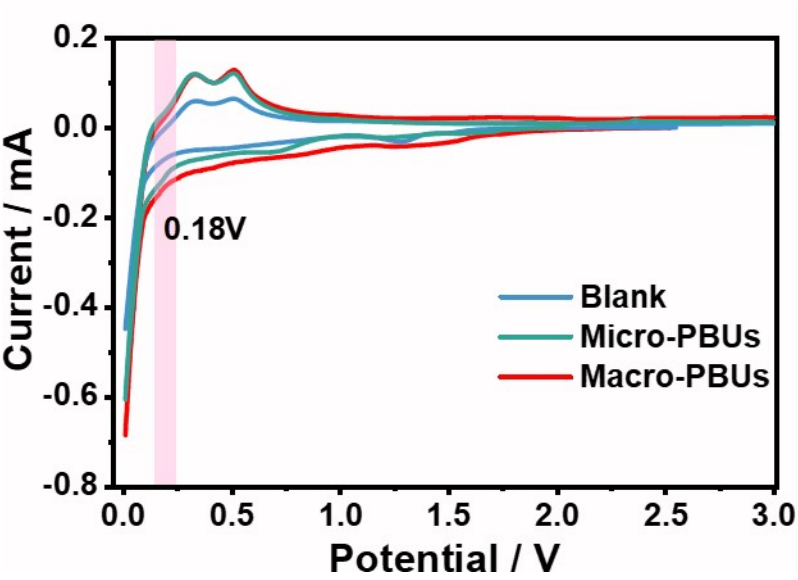

Fig. S8. CV curves of Macro-PBUs, Micro -PBUs, and Blank at a scan rate of 0.2 mV s^{-1},

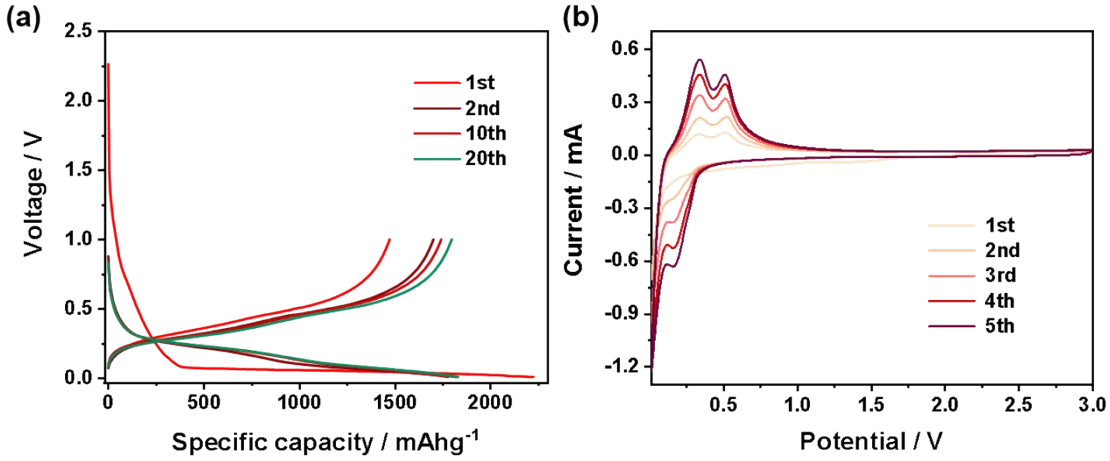

Fig. S9. (a) GCD curves of Macro-PBUs electrode, (b) CV curves of Macro-PBUs electrode at a scan rate of 0.2 mV/s.

As shown in Fig. S9a, the GCD curves of Macro-PBUs tends to be stable with the process of charge/discharge and specific capacity further increases after activation, which is consistent with the results shown in CV curve of Fig. S9b.

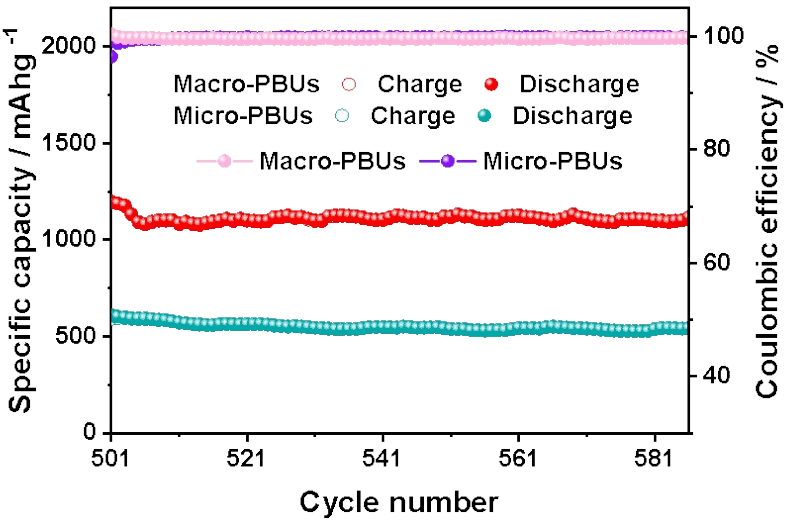

Fig. S10. The cycling performances of electrodes after 500 cycles at a current density of 1 A g^{-1}

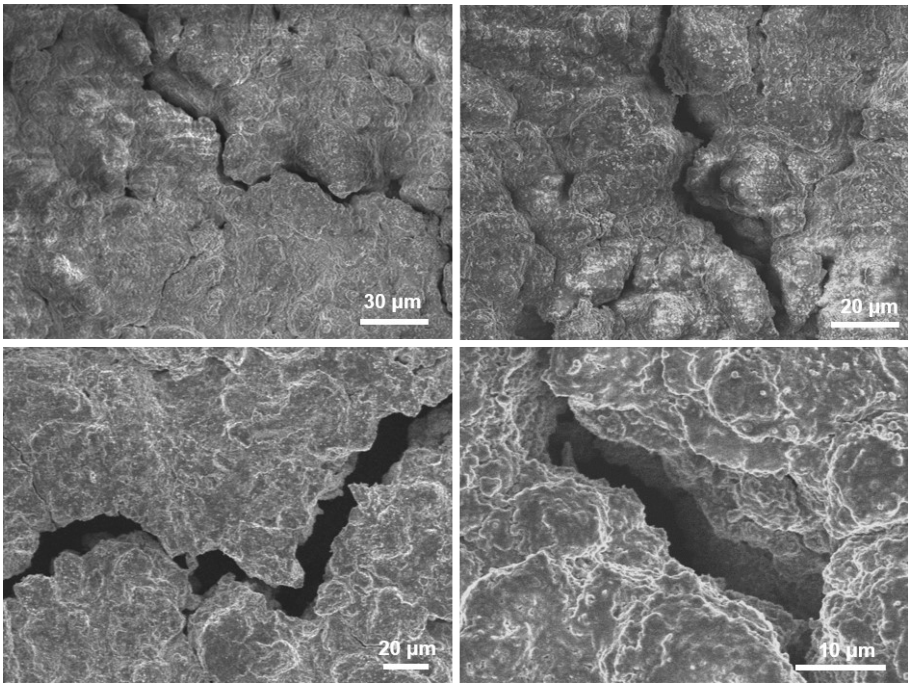

Fig. S11. SEM images of Micro-PBUs electrode after cycling.

The morphology of Micro-PBUs disk after cycling was characterized by SEM. As displayed in Fig. S11, Micro-PBUs disk exhibit a noticeable crack and a rough surface after 500 cycles. The width of the crack is close to 10 μm.

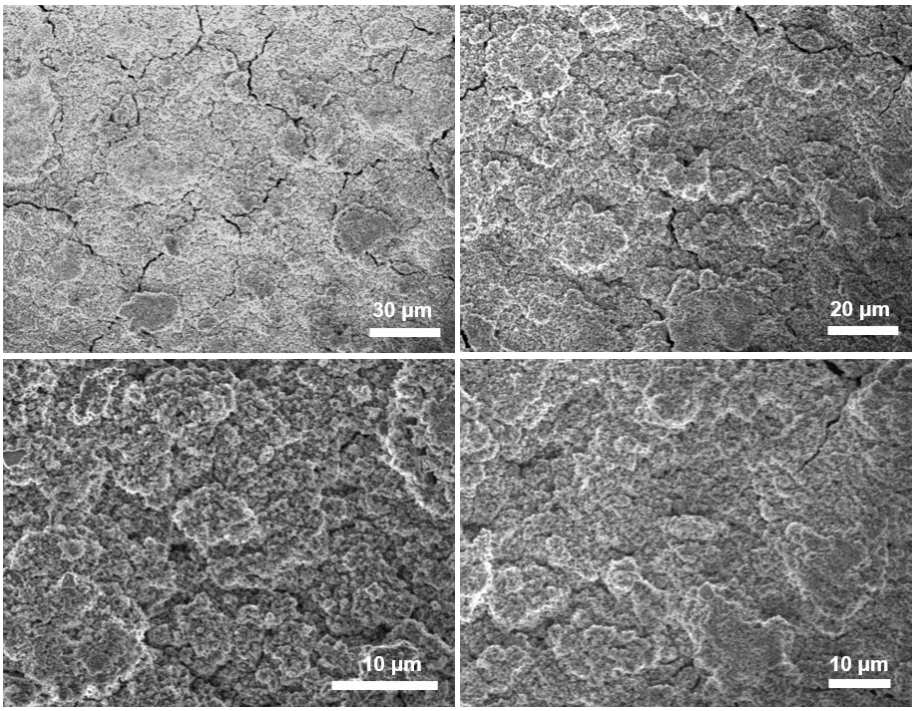

Fig. S12. SEM images of Macro-PBUs electrode after cycling.

The morphology of Macro-PBUs disk after cycling was also characterized by SEM. As displayed in Fig. S12, only some slight cracks were observed on the surface of the Macro-PBUs electrode disk, indicating that secondary cross-linking network and MX help to enhance the resistance capability to volume change and maintain the integrity of the electrode structure.

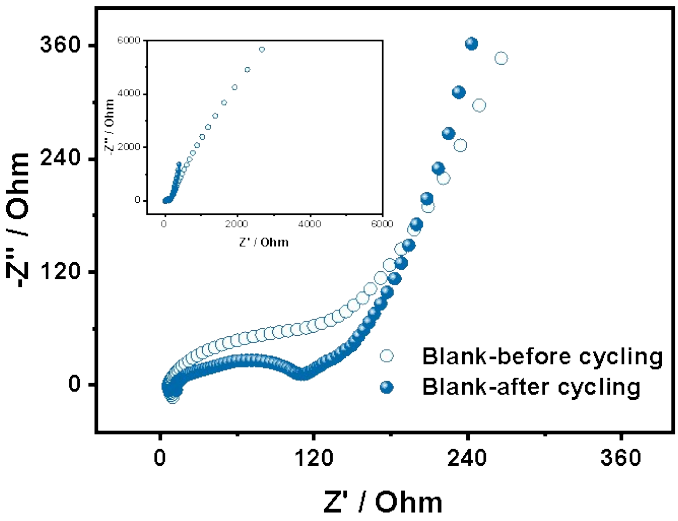

Fig. S13. Nyquist plots of Blank electrode before and after cycling

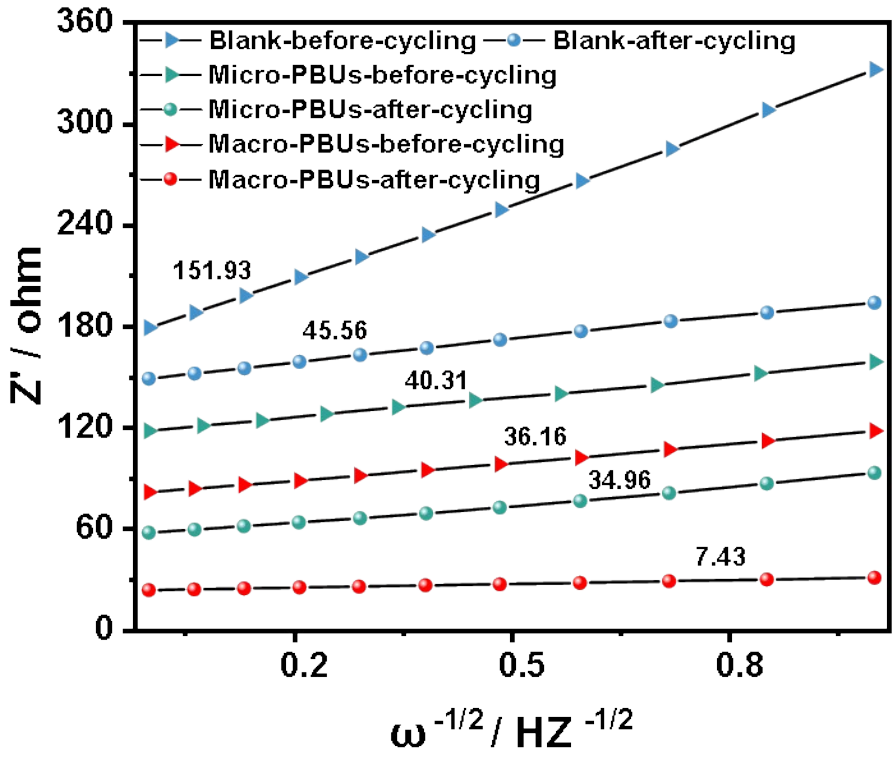

Fig. S14. Diffusion coefficient of Blank, Micro-PBUs, Macro-PBUs electrodes before and after cycling.

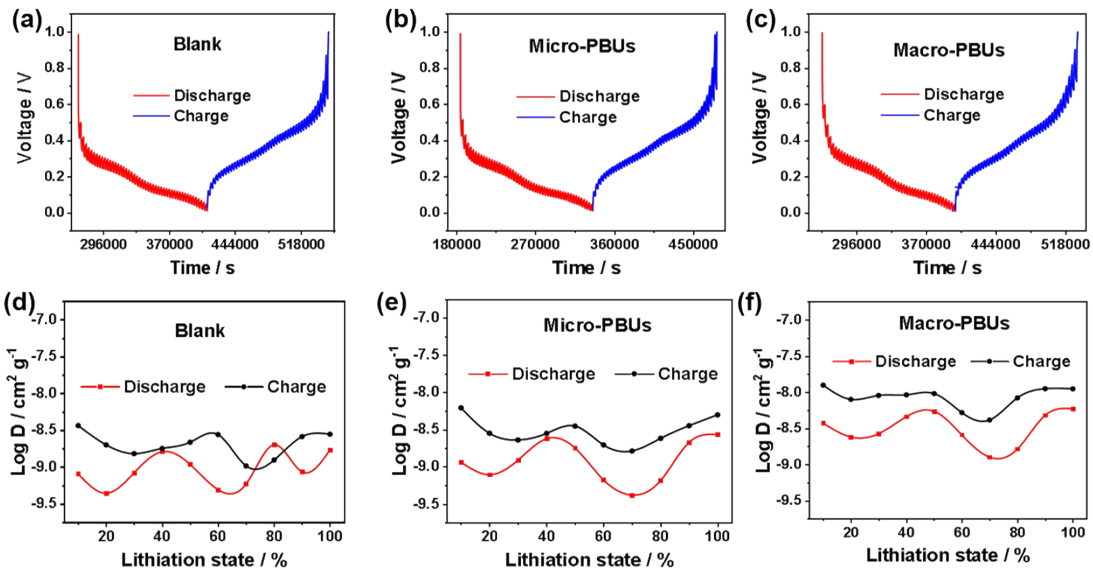

Fig. S15. (a-c) GITT curves of Blank, Micro-PBUs and Macro-PBUs electrodes with a pulse current density of 100 mA g^{-1}, (d-f) Corresponding ions diffusion coefficients of Blank, Micro-PBUs and Macro-PBUs electrodes.

As shown in Fig. S15, we observed that the Li^+ diffusion coefficient during charge process is obviously higher than that during the discharge process. This finding suggests that the extraction process of Li^+ is faster than the insertion process. In addition, the Macro-PBUs electrode consistently delivers a higher Li^+ diffusion coefficient when compared to both Micro-PBUs and Blank electrode over the entire charging/discharging process. The higher Li^+ diffusion coefficient can mainly be ascribed to the construction of dual cross-linked networks and the introduction of MX.

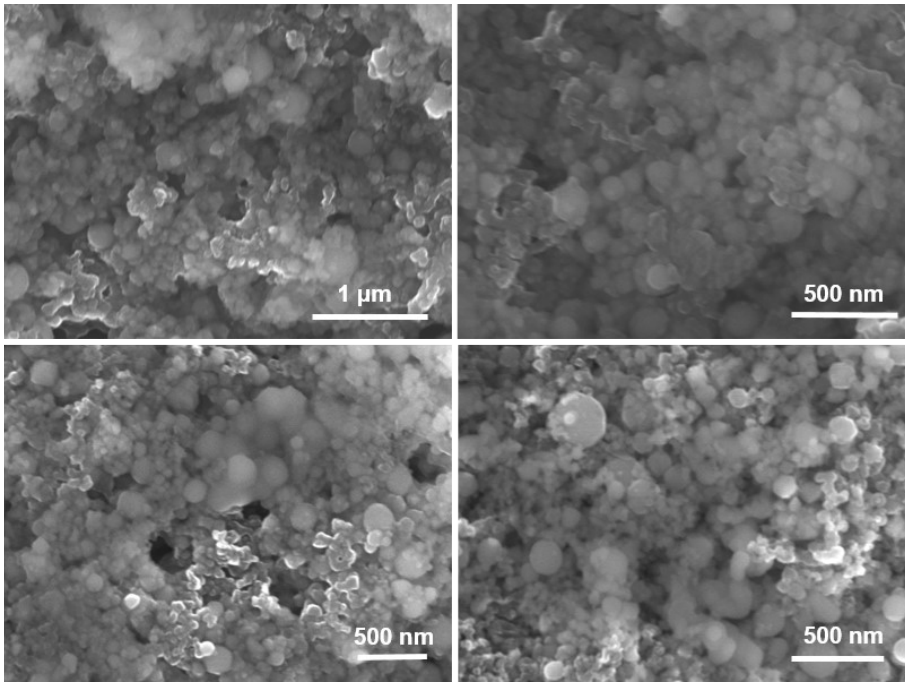

Fig. S16. SEM images of Macro-PBUs-W-MX electrode.

To explore the role of MX in electrode structure, secondary solidified particles without mxene (Macro-PBUs-W-MX) was fabracted and subjected to SEM testing. As shown in Fig. S16, Macro-PBUs-W-MX displays a relatively uniform particle morphology, with the larger particles being silicon particles and the smaller particles dispersed around Si being AB particles. The morphology of Macro-PBUs-W-MX is similar to that of Micro-PBUs.

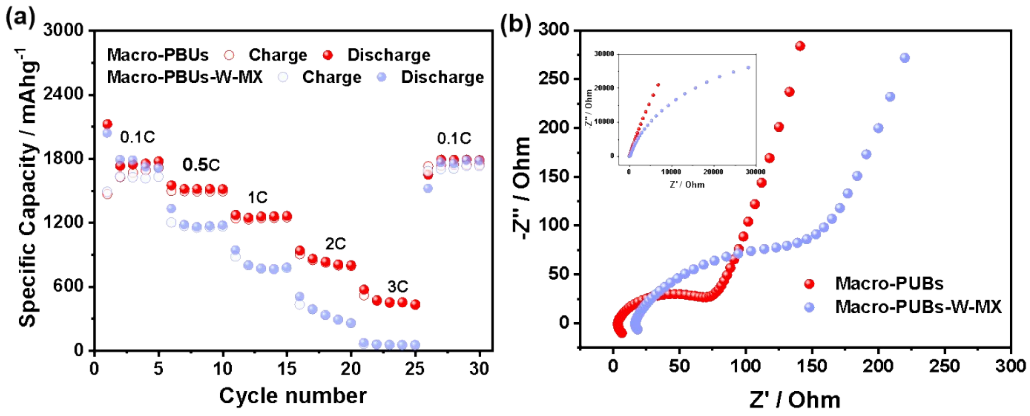

Fig. S17. (a) Rate performances of Macro-PBUs and Macro-PBUs-W-MX electrodes, (b) Nyquist plots of Macro-PBUs and Macro-PBUs-W-MX electrodes.

To further prove that the addition of MX can effectively improve the charge transfer ability, rate performances was conducted. As shown in Fig. S17a, Macro-PBUs show the better rate performance compared with Macro-PBUs-W-MX. Due to the introduction of MX, Macro-PBUs formed 3D conductive framework structure, which significantly improve the rate performance. As shown in Fig. S17b, the electron conductance and ion diffusion of Macro-PBUs are noticeable improved. Compared to Macro-PBUs-W-MX electrode, Macro-PBUs show a smaller charge transfer impedance and ion diffusion impedance.